Resource-Efficient Technologies 2 (2020) 16–24

TOMSK POLYTECHNIC UNIVERSITY

Resource-Efficient Technologies

journal homepage: http://reffit.tech

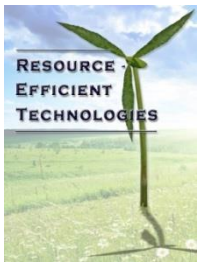


Review Paper

# PHYTOMEDIATED SYNTHESIS OF SILVER NANOPARTICLES AGAINST MICROBIAL PATHOGENS AND CYTOTOXICITY ON HUMAN BREAST CANCER CELLS (MCF-7)

Karthiga P., Shankar T., Karthick K., Swarnalatha K.*

Photochemistry Research Laboratory, Department of Chemistry,
Manonmaniam Sundaranar University, Abishekapatti, Tamil Nadu, India.

## Abstract

Silver nanoparticles (AgNPs) are synthesized from the root extract of the *Abutilon indicum plant*. Nitrate reductase enzyme and/or other extra cellular proteins released from the extract reduce the silver nitrate to silver ions. These proteins or enzymes serve as a template for the silver nucleation sites in the development of silver nanoparticles, and also act as capping agents, preventing silver ion agglomeration. XRD analysis predicts the phase of the nanoparticles. Transmission Electron Microscope (TEM) and Scanning Electron Microscope analyses have revealed that the synthesized AgNPs are spherical in shape, with an average size of 17 nm. From the data, it is noted that the protein molecules and fatty acids present in the root extract of *Abutilon indicum*, play a vital role in reducing silver salts and as capping AgNPs at various concentrations. Bactericidal activity acting against the clinical pathogens was performed, and it was observed that NP inhibition is highly dependent on their size and surface. Cytotoxic studies were carried out with these synthesized silver nanoparticles using MTT assay on MCF-7 cells.

*Keywords:* Abutilon indicum, root extract, nanosilver, pH, bactericidal activity, MCF-7 cells.

## 1. Introduction

Nanoparticles (NPs) have attracted significant global interest for their potential application in various fields, including drug delivery, diagnostics, tissue engineering, parasitological usages, and also in many clinical and environmental applications, due to their unique physical and chemical properties [1, 2]. Bio/green synthesis of nanoparticles has received considerable attention, as they are non-toxic and more advantageous as compared to physical and chemical synthesis. At present, diverse types of metal nanoparticles are being formed, including copper, zinc, titanium, magnesium, gold, and silver, by diverse techniques including sono-chemical, spray pyrolysis, and hydrothermal. However, recently, biosynthesis of nanoparticles via bacteria, fungi, and plants has emerged as an easy and viable alternative to the complex physical and chemical synthetic methods for obtaining target nanoparticles [3]. Research in nanotechnology, especially for green chemistry pathways to fabricate technologically important nanomaterials, is an immense area of interest [4].

In recent decades, new methods, based on applications of photodegradation, appeared promising [5]. Plants, bacteria, fungi, and algae have all been used for the green synthesis of metal nanoparticles in aqueous media [6]. Synthesizing nanoparticles via biological entities acting as biological factories offers a clean, non-toxic, eco-friendly method of synthesizing nanoparticles that offer a wide range of sizes, shapes, compositions, and physicochemical properties [7]. In comparison with microorganisms,

* Corresponding author: Swarnalatha Kalaiyar
E-mail: swarnalatha@msuniv.ac.in

☆Peer review under responsibility of Tomsk Polytechnic University.
https://doi.org/10.18799/24056537/2020/1/235

plant-mediated biological methods have attracted much attention due to the necessity of developing new, clean, cost-effective, and efficient synthetic techniques. Recently, many biological systems, such as bacteria, yeast, fungus, and several plant extracts, have been used as reducing agents in the reduction of metal ions to form nanoparticles. Synthesis of nanoparticles employing plants can likely render more biocompatibility to the nanoparticles. Furthermore, synthesis using plants tends to be faster than using microorganisms, and is comparatively easy to scale up for the production of enormous quantities of nanoparticles [8, 9]. Synthesis of NPs by plant extracts prevents the use of capping agents to yield size- and shape-dependent products. The precise mechanism for shape-control of silver and gold nanoparticles by biological means is not clear; The option of achieving NPs of different shapes by using different plant parts appears to be a better alternative. A number of approaches are accessible for the synthesis of silver nanoparticles, For example, reduction in solutions, thermal decay of silver compounds, radiation-assisted, electrochemical, sono-chemical, microwave-assisted processes, and phyto-assisted routes. These approaches have numerous benefits over chemical, physical, and microbial synthesis, as there is no need for the detailed process of culturing the cell or for toxic chemicals [10, 11].

Plants provide natural capping agents; additionally, the use of plant extracts also reduces the price of microorganisms, isolation, and culture media, enhancing the "reasonable cost" possibility over nanoparticles synthesized by microorganisms. Some reports established that the antibacterial activities of AgNPs are dependent on the size and shape of the nanoparticles. The antibacterial activity increases with a decreasing size of Ag NPs. Aggregation of nanoparticles causes less effect in the antibacterial activity of Ag NPs. The rate of reduction of metal ions using plants has been found to be much faster as compared to microorganisms, and constant formation of metal nanoparticles has been reported. The shape and size of the nanoparticles synthesized using plants can be controlled and modulated by altering the pH [12, 13].

It is well known that Ag ions and Ag-based compounds are very noxious to microbes and cell lines, showing strong biocidal and cytotoxic effects. Herein, we have explored the toxicity studies of synthesized silver nanoparticles using *A. indicum* root extract at different pH conditions.

## 2. Materials and Methods

### 2.1. Materials

Silver nitrate ($AgNO_3$, 99.9 %), potassium bromide (KBr), sodium hydroxide (NaOH) were purchased from Merck Limited. Nutrient Agar, Nutrient Broth, Agar Agar, Muller-Hinton Agar (MHA) were obtained from Himedia Laboratories. DMEM (Dulbecco's Modified Eagle's Medium), Fetal Bovine Serum (FBS), and antibiotic solution were from Gibco (USA), DMSO (Dimethyl sulfoxide) and MTT (3-4,5 dimethylthiazol-2yl-2,5-diphenyl tetrazoliumbromide) (5 mg/ml) were from Sigma, (USA), 1X PBS was from Himedia, (India). 96 well tissue culture plate and wash beaker were from Tarson (India). The plant, *Abutilon indicum* belonged to Malvaceae family and the common name is Thutti. Fresh roots of *Abutilon indicum* were collected in Manonmaniam Sundaranar University Campus, Tirunelveli, Tamil Nadu.

### 2.2. Preparation of Root Extract

Freshly collected roots (Figure 1) were thoroughly washed under running tap water in order to remove the dust and other particles adhering to the surface, and then rinsed well with distilled water. The surface-cleaned roots were chopped into small pieces and mixed with 100 ml of sterile distilled water, then boiled at 80 °C for 15 minutes. The combination was chilled to room temperature and filtered through Whatman No. 1 filter paper. The obtained root extract (yellow color) was stored at 4 °C and used for the synthesis of silver nanoparticles.

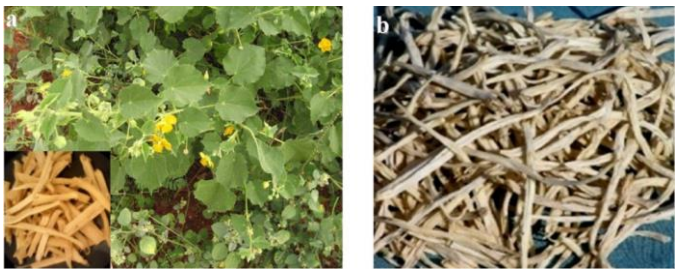


**Fig. 1.** *Abutilon indicum* (a) plant and (b) fresh roots.

### 2.3. Synthesis of Silver Nanoparticles

12 ml of the root extract was mixed with 88 ml of 1 mM silver nitrate solution and stirred for 15 minutes at room temperature. A color change from straw yellow to brown was observed, indicating the formation of silver nanoparticles. In order to study the surface structure and reactivity of the silver nanoparticles synthesized from root extract, the

experiments were repeated with different concentrations of silver nitrate solution (1, 2, 3, 4 & 5 mM) and at different pH levels (4.5, 6.5, 8.5 & 10.5).

### 2.4. Instrumentation

The crystalline character of the synthesized silver nanoparticles was examined with the help of powdered XRD, using Panalytical X'pert Powder X'Celerator diffractometer. The X-ray patterns were obtained in two theta configurations, in the range of 20°–80°. After drying off the purified silver nanoparticles, the elemental composition of the sample was analyzed with energy dispersive analysis of X-ray spectroscopy (EDS, Sigma). The surface and size were analyzed using a Scanning Electron Microscope (SEM, Hitachi S-2500C) and Transmission Electron Microscope (TEM, Jeol /JEM 2100). Absorption spectra were recorded on a Perkin Elmer Lambda 25 double beam spectrophotometer in the wavelength range of 200 nm to 800 nm, with a 1 cm path length quartz cuvette. In cytotoxic activity, the quantity of formazan product, was measured at 570 nm using a micro plate reader (Thermo Fisher Scientific, USA)

### 2.5. Bactericidal Activity

The synthesized AgNPs were tested for antimicrobial activity by the agar well-diffusion method [14] against different varieties of pathogenic bacteria isolated from clinical samples: *Bacillus subtilis*, *Staphylococcus aureus* (Gram-positive bacteria) *Escherichia coli, Klebsiella pneumonia* (Gram-negative bacteria). A fresh overnight culture of each strain was swabbed uniformly onto the individual plates containing sterile MHA with a sterile cotton swab; wells of 6 mm diameter were bored into the agar medium using gel puncture. Using a micropipette, 100 ▫l of the Ag NPs and root extracts were added into each well. Inoculated Petri dishes were incubated for 24 hours at 37°C. Following incubation, different levels of the zone of inhibition which formed around the well were measured. Filtrate (plant extract) was used as the negative control. The experiments were performed in triplicate.

### 2.6. Cell Culture

The MCF-7 cell line was cultured in liquid medium (DMEM), supplemented with 10 % FBS, 100 u/ml penicillin and 100 µg/ml streptomycin, and maintained under an atmosphere of 5 % $CO_2$ at 37 °C.

### 2.7. MTT Assay

The sample was tested for *in vitro* cytotoxicity, using MCF-7 cells by 3-(4,5-dimethylthiazol-2-yl)-2,5-diphenyltetrazolium bromide (MTT) assay [15]. Briefly, the cultured MCF-7 cells were harvested by trypsinization, and pooled in a 15 ml tube. Then, the cells were plated at a density of $1 \times 10^5$ cells/ml cells/well (200 µL) into a 96-well tissue culture plate in DMEM medium containing 10 % FBS and 1 % antibiotic solution for 24–48 hour at 37 °C. The wells were washed with sterile PBS and treated with various concentrations of the sample in a serum-free DMEM medium. Each sample was replicated three times, and the cells were incubated at 37 °C in a humidified 5 % $CO_2$ incubator for 24 hours. After the incubation period, MTT (20 µL of 5 mg/ml) was added into each well and the cells incubated for another 2–4 hours, until purple precipitates were clearly visible under an inverted microscope. Finally, the medium, together with MTT (220 µL), was aspirated off the wells and washed with 1X PBS (200 µl). Furthermore, in order to dissolve formazan crystals, DMSO (100 µL) was added and the plate was shaken for 5 minutes. The absorbance for each well was measured at 570 nm using a micro plate reader (Thermo Fisher Scientific, USA) and the percentage cell viability and IC50 value were calculated using GraphPad Prism 6.0 software (USA).The relative cell viability (%) related to control wells containing cell culture medium without nanoparticles as a vehicle was calculated according to the formula,

$$\text{Cell viability (\%)} = \text{Mean OD/control OD} \times 100 \quad (1)$$

$$\text{Cytotoxicity (\%)} = 100 - \text{cell viability \%} \quad (2)$$

## 3. Results and Discussion

### 3.1. Visual Examination and Spectral Features

Initially, the reaction mixture exhibited no color change, turning brown after 10 minutes of incubation. The structural variation of the particles was examined by the UV-Visible absorption spectrum, which assists in evaluating the complex formation. It is the primary method for indicating the bioreduction of silver from aqueous silver nitrate solution to silver nanoparticles. The brown color indicated that the process of silver nanoparticles production had begun; the intensity of the brown color increased after 24 hours. After 24 hours, the settling of

synthesized silver nanoparticles at the bottom of the vessel revealed that the reduction of silver metal into silver nanoparticles was complete (Figure 2). The schematic route for phyto-synthesis is provided in Figure 3. Similar color observations were noted in the plant extracts of *Acalpha indica* and *Calliandra haematocephala* [16, 17].

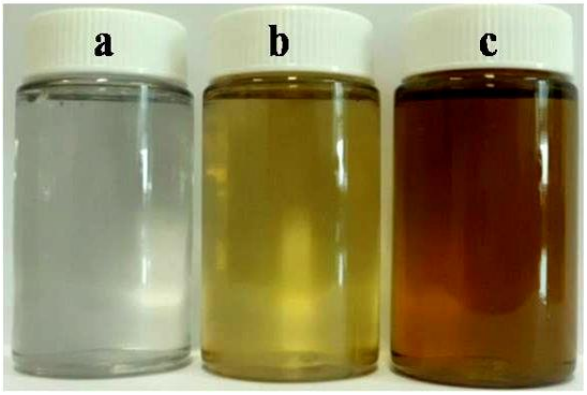


**Fig. 2.** Visual identification of silver nanoparticles (a) $AgNO_3$ solution, (b) root extract and (c) Ag NPs

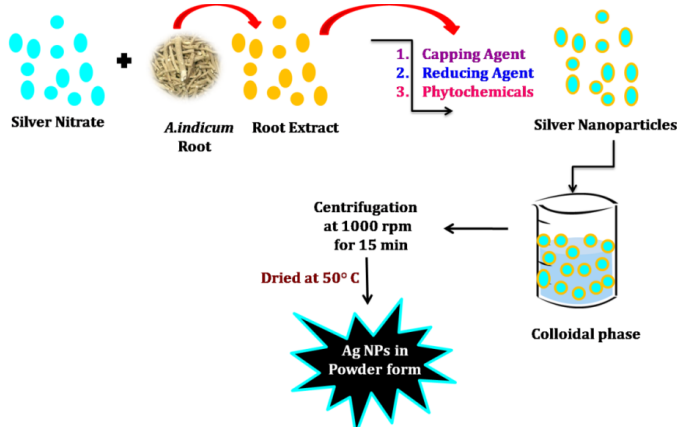


**Fig. 3.** Schematic representation of phytomediated synthesis of Ag NPs

### 3.2. Effect of $AgNO_3$ Concentration

To study the optimal parameters for silver nanoparticles synthesis, the experiments were carried out at different concentrations of silver ions (1, 2, 3, 4, and 5 mM), presented in Figure 4. The optical absorption spectra of metal nanoparticles were dominated by the surface plasmon resonance (SPR), which displayed a shift toward the red end or blue end, depending upon the particle size, shape, state of aggregation, and the surrounding dielectric medium [18]. After 24 hours, the settling of silver nanoparticles to the bottom of the Erlenmeyer flask revealed that the reduction of silver metal into silver nanoparticles was complete. Different concentrations of silver nitrate were carried out to synthesize silver nanoparticles in order to find the optimum concentration. Among these, 1 mM showed the band at 440 nm, which may be due to the various fatty acids present in the root extract. The secondary metabolites and other antioxidants present in the root extract served both as reducing and capping agents to form the nanoparticles. The decrease of silver ions and the growth of nanoparticles occurred in 30 minutes, due to excitation of surface plasmon vibrations in the nanoparticles. On increasing the concentration from 2 to 5 mM, the particles became highly aggregated with one another.

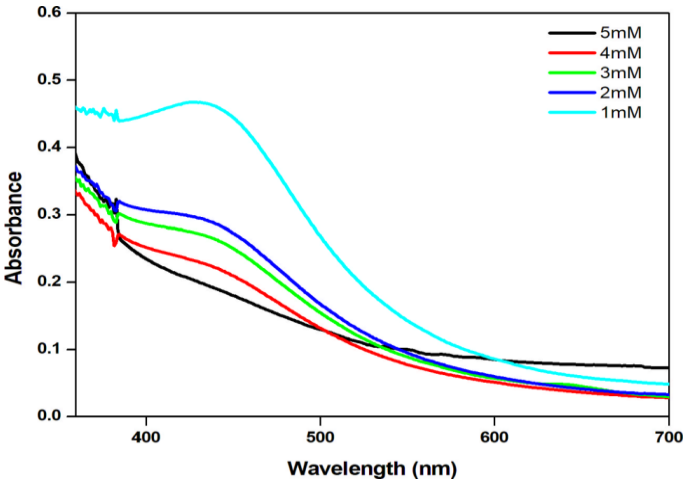


**Fig. 4.** Absorption spectra of silver nanoparticles from different metal ion concentration (1, 2, 3, 4 and 5 mM)

### 3.3. Effect of pH

Studies have demonstrated that varying the pH of the reaction medium tends to cause variability in the shape and size of the synthesized nanoparticles. During the phyto-mediated synthesis of silver nanoparticles using root extracts, a mixture of constituents may contribute to the reduction process of silver ions. Therefore, altering the chemical state (e.g., ionization) of these constituents can affect the performance and rate of the reduction process. For this reason, the effect of pH (4.5, 6.5, 8.5, and 10.05) on the synthesis of Ag NPs was investigated by using a UV-Vis spectrophotometer. The results, shown in Figure 5, suggested that the rate of silver nanoparticle synthesis increased with an increasing pH (up to pH = 10.05 marked as S1, S2, S3, and S4). The reason for this behavior may be due to the ionization of phenolic compounds and tannins in the extract of *Abutilon indicum* [19, 20, 21, 22]. This study suggested that more available functional groups are contained in the extract when the pH is between 8.5 and 10.5; these are responsible for particle nucleation. On the other hand, at a pH less than 4.5, fewer functional groups were available and resulted in particle aggregation, forming larger silver nanoparticles.

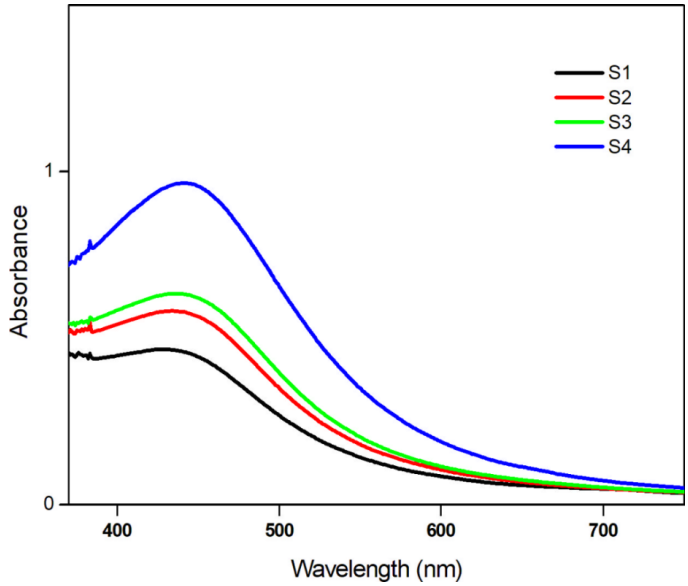


**Fig. 5.** Absorption spectra of silver nanoparticles synthesized from different pH = 4.5, 6.5, 8.5 10.5 marked as (S1, S2, S3 and S4)

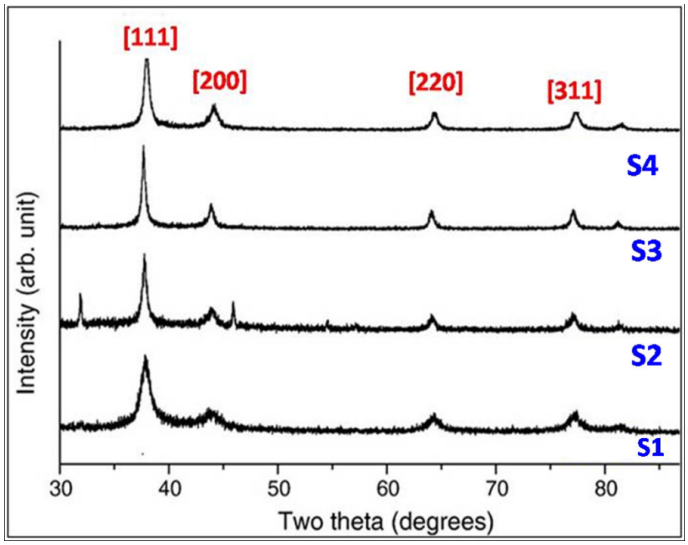


**Fig. 6.** X-ray diffraction patterns of the prepared silver nanoparticles. Labeled peaks correspond to the characteristic diffraction peaks of elemental Ag (0) (pH = 4.5, 6.5, 8.5 10.5)

### 3.4. X-ray Diffraction

The crystalline nature of silver nanoparticles was confirmed from XRD analysis. Figure 6 shows the XRD pattern of Ag NPs obtained using the root extract of *A. Indicum*. The diffraction peaks appeared at 38.3°, 44.6°, 64.8°, and 77.9, and correspond to the (111), (200), (220), and (311) facets of the face-centered cubic crystal structure, respectively. The average crystallite size according to Scherrer's equation, calculated using the width of the (111) peak, is found to be 15–17 nm nearly in agreement with the particle size obtained from TEM image of S3. The obtained XRD patterns were compared and coordinated with the joint committee powder diffraction standards JCPDS file No. 04–0783. It should be mentioned that the unassigned peaks are owing to the crystallization of bioorganic phases that happen on the outside of the silver nanoparticles.

### 3.5. SEM–EDX

The results of SEM analysis demonstrated that the average sizes of nanoparticles were 40 nm and 17 nm. The UV-Vis spectra of the silver nanoparticles were maintained at different pH levels as S1, S2, S3, and S4. The surface plasmon resonance (SPR) band indicates monodispersed nanoparticles. As the pH was increased, the SPR band sharpened in basic conditions at a pH of 10.05, which was clearly confirmed in absorption spectra of pH. The spectra showed a smooth and narrow band at 440 nm, indicating the monodispersed nanoparticles. The broad SPR band observed at lower pH values were due to the large anisotropic particles. The SEM image obtained for S1 and S3 are shown in Figures 7 and 8. It was clear from the SEM images that the particle size decreases as the pH is increased, and at last, in S3, the average size of the particle was 17 nm. The results of EDX analysis is predicted in Figure 9. The EDX profile showed a strong silver signal at 3 KeV, which predicted the binding energy of AgL. This proved the confirmation of pure silver due to the surface plasmon resonance. Presence of weak oxygen and carbon peaks in the EDX graph are originated from the bio-molecules that were bound to the surface of the AgNPs.

### 3.6. Transmission Electron Microscope

The TEM image of silver nanoparticles, shown in Figure 10, signifies that the synthesized silver nanoparticles are monodispersed. The image with clear lattice fringes reveals that the growth of silver nanoparticles occurred preferentially on the (111) plane. In lower pH, the growth was favored due to the absence of fatty acids. The broadening of the SPR band indicated the larger size nanoparticles, as evidenced in UV-Vis spectra. In a higher pH environment, due to the addition of sodium hydroxide, various fatty acids viz. linoleic, oleic, stearic, palmitic, lauric, myristic, caprylic, capric, and unusual fatty acid having $C^{17}$ carbon skeleton and amyrin from unsaponifiable matter, were yielded [17], which in turn resulted in the reduction of silver ions and formed a large number of very small nanoparticles,

at 12 nm in size. This gave rise to a sharp and intense SPR band. The synthesized silver nanoparticles were spherical in shape. Some undefined shapes were also observed due to slight nucleation.

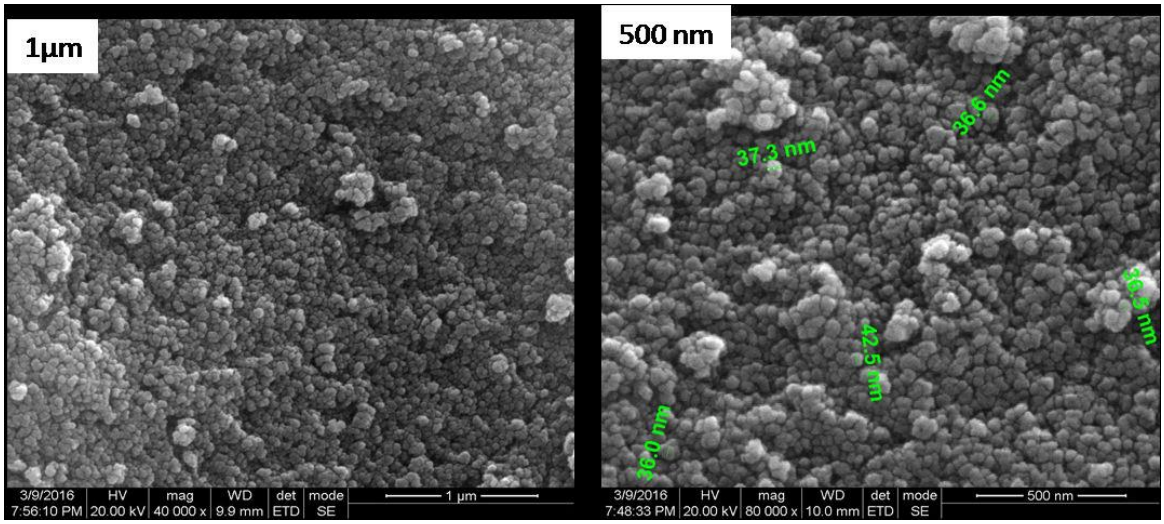


**Fig. 7.** SEM micrograph of silver nanoparticles (S1) at pH=4.5

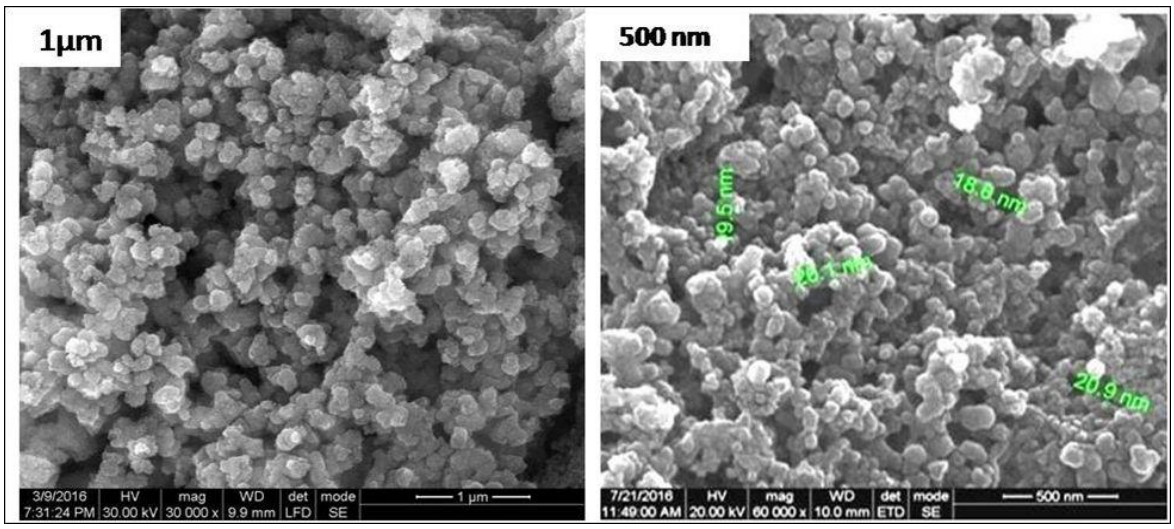


**Fig. 8.** SEM images of silver nanoparticles (S3) at pH= 8.5

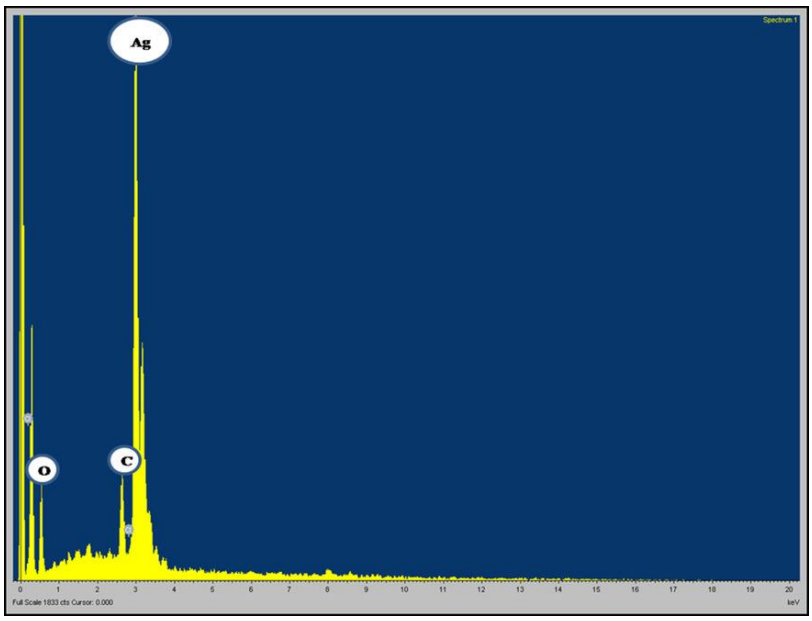


**Fig. 9.** EDX profile of the synthesized silver nanoparticles

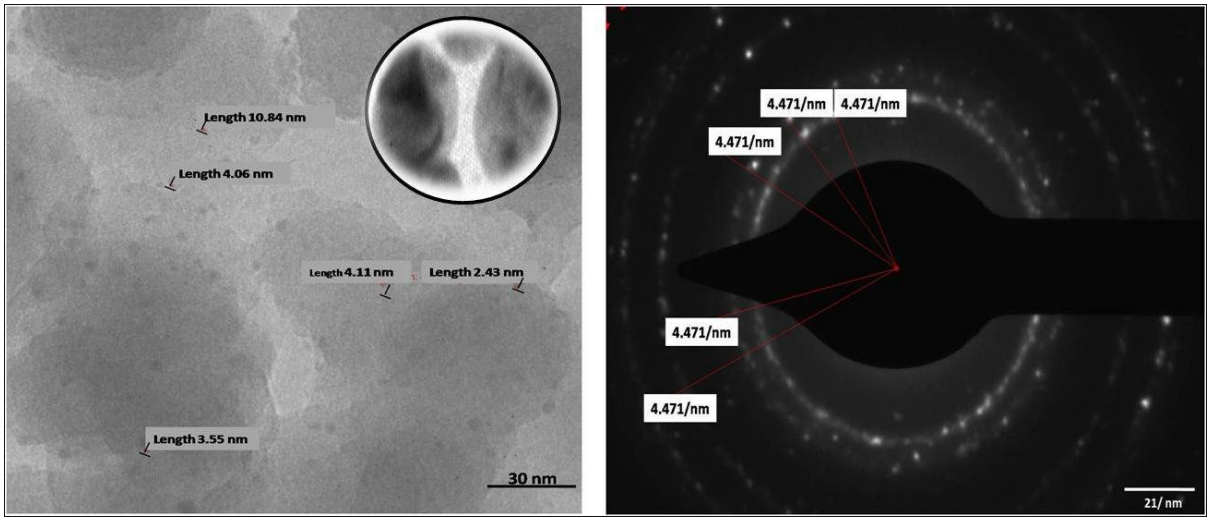


**Fig. 10.** TEM and SAED micrograph of silver nanoparticles (S3) at pH= 8.5.

3.7. Bactericidal Activity

It has been known, over the last few decades, that chemical groups are present in essential oils, which are capable of much antibacterial activity; this is both a safe and effective therapy against various antimicrobial agents [23]. The synthesized nanoparticles inhibit bacterial growth against mainly gram-negative strains, and to a lesser extent in gram-positive microbes. Both gram-positive bacteria (*B. Subtilis, S. Aureus*) and gram-negative bacteria (*E. Coli, K. Pneumonia*, and *P. aurogenosa*) demonstrated zones of growth inhibition, clearly depicted in Figure 11.

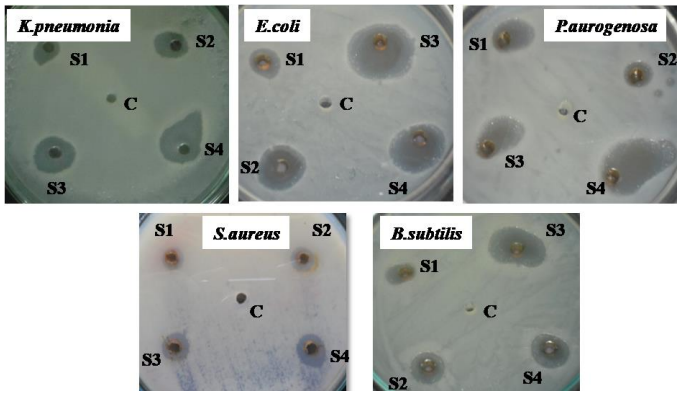


**Fig. 11.** Microbial activity of silver nanoparticles (100 µl) against test organisms

Compared to gram-positive organisms, gram-negative bacteria displayed a maximum zone of inhibition (Figure 12), and the possible mode of action is shown in Figure 13. There were diverse possibilities for silver NPs to disturb the biological system. Silver nanoparticles and soluble silver salts released the silver ions when they came in contact with water. These ions were biochemically active agents [24, 25], and will react with sparingly soluble salts, which remain in colloidal dispersion, also undergoing complexation with other bio-molecules.

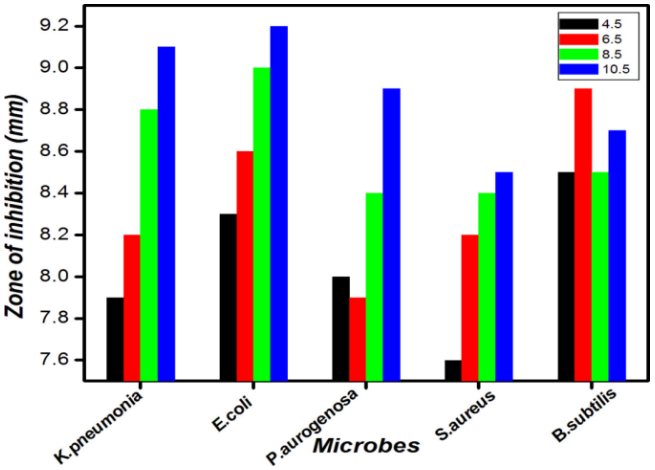


**Fig. 12.** Antibacterial assay of *A. indicum* root extract and silver nanoparticles against gram-positive and negative microbes

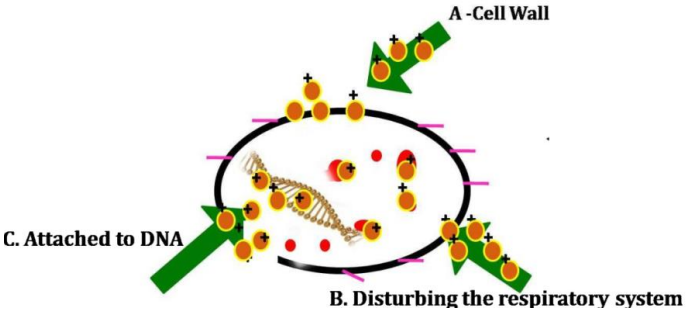


**Fig. 13.** Possible mechanism of the formation of zone of inhibition

Smaller AgNPs possess a higher toxicity than larger silver nanoparticles. With smaller-sized particles, as with a higher pH (basic), the zone of inhibition enlarges. In the case of a lower pH (acidic), a larger particle size was produced due to the agglomeration. In lower pH, hydrochloric acid also plays a

vital role, as this acid may cause chemical alterations in the extract. As reported earlier, secondary metabolites reacted with the acid and produced the agglomeration in the particles. This leads to the variations in the zone of inhibition [26, 27].

This can partially be explained by the facilitated invasion of smaller-sized nanoparticles into the cell wall of gram-negative bacteria, which consists of a distinct outer membrane layer and a single peptidoglycan. However, in gram-positive bacteria, the cell wall consists of numerous peptidoglycan layers; therefore its cell wall is more exposed to nanoparticles through the surface bacterial membrane. The larger surface area of chitosan-copper nanoparticles enables them to interact with the bacterial cell membrane through its surface, leading to bacterial death [28]. The above-mentioned possible mechanism is also fitting for silver nanoparticles, which lead to the death of microbial pathogens. Thus, the size of the nanoparticles is important for bactericidal activity.

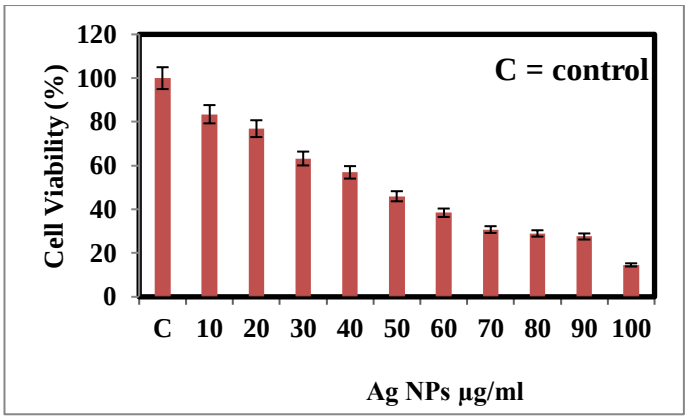


**Fig. 14.** Percentage of Cell viability against silver nanoparticles (S3)

### 3.8. Cytotoxic Assay

AgNPs synthesized using plant extract was tested for its cytotoxic effect using MTT on an MCF-7 cell line. Biosynthesized AgNPs, of varying concentrations in cell lines, were tested following 24 hours of incubation at 37 °C in 5 % $CO_2$. The present study examined the effect of root extracts of *A. indicum* on MCF-7 cells survival using the MTT test.

Twenty-four hours after seeding the cells into 96 well microliter plates, the effect of 10, 30, 50 and 100 µg/ml of *A. indicum* extract mediated Ag NPs on cell growth was analyzed [29–31]. When compared to the other concentrations, the Ag NPs at a concentration of 100 µg/mL exhibited a significant toxic effect. Figure 14 shows the cell viability for the control and the sample at 570 nm. Ag NPs produce a significant cytotoxic effect at concentrations of 100 µg/ml.

## 4. Conclusion

We have successfully synthesized silver nanoparticles via a pH-induced phytomediated pathway. The effect of silver ion concentration, pH, and root extract concentration on the size of the silver nanoparticles were investigated. Phytomediated synthesis of AgNPs in varying pH media demonstrated a strong inhibition against gram-positive and gram-negative microbes. The cytotoxic activity of cells (MCF-7) is triggered by AgNPs, depending on the concentration. Current work reported that the *A. indicum* plant-based spherical shaped nanoparticles, with a size of 17 nm, were produced in a basic pH condition, with remarkable antibacterial and cytotoxic activities. The results present important features of AgNPs, with significant antibacterial and cytotoxic activity, in order to attain selected goals in the therapeutic applications.

## Acknowledgment

This work was supported by the University Grants Commission, New Delhi, (Ref No: F. 15-1/2012-13/PDFWM-2012- 13-SC-TAM-21783**)** (SA-II)–dated 18.04.2014. Also we thank Dr. G**.** Annadurai**,** Professor, Centre for Environmental Sciences, Azhwarkurichi, for providing the laboratory facility for biocidal studies.

## References

[1] Benelli G., Lukehart C.M. Special Issue: Applications of green-synthesized nanoparticles in pharmacology, parasitology and entomology. *J Clust Sci*, 2017, vol. 28, no. 1, pp. 1–2. doi:10.1007/s10876-017-1165-5.

[2] Benelli G. Gold nanoparticles–against parasites and insect vectors. *Acta trop*, 2018, vol. 178, pp. 73–80. doi: 10.1016/j.actatropica.2017.10.021.

[3] Mallikarjuna K., *et al*. Green synthesis of silver nanoparticles using Ocimum leaf extract and their characterization. *Digest J Nanomat and Biostruct*, 2011, vol. 6, no. 1, pp.181–186.

[4] Baskaralingam V., Sargunar C.G., Lin Y.C., Chen J.C. Green synthesis of silver nanoparticles through Calotropis gigantean leaf products and evaluation of antibacterial activity against Vibrio alginolyticus. *Nanotechnol Dev*, 2012, vol. 2, no. 1, pp. 12–16. doi: 10.4081/nd.2012.e3.

[5] Kalaiselvi A., Roopan S.M., Madhumitha G., Ramalingam C., Elango G. Synthesis and characterization of palladium nanoparticles using Catharanthus roseus leaf extract and its application in the photo-catalytic degradation.

*Spectrochim Acta – PartA: Molecular and Biomolecular Spectroscopy*, 2015, vol. 135, pp. 116–119. doi:10.1016/j.saa.2014.07.010.

[6] El-Faham A., Elzatahry A.A., Al-Othman Z.A., Elsayed E.A. Facile method for the synthesis of silver Nanoparticles using 3-hydrazino-isatin derivatives in aqueous methanol and their antibacterial activity. *International Journal of Nanomedicine*, 2014, vol. 9, no. 1, pp. 1167–1174. doi:10.2147/IJN.S58571.

[7] Mohanpuria P., Rana N.K., Yadav S.K. Biosynthesis of nanoparticles: technological concepts and future applications. *Journal of Nanoparticle Research*, 2008, vol. 10, no. 3, pp. 507–517. doi:10.1007/s11051-007-9275-x.

[8] Iravani S. Green synthesis of metal nanoparticles using plants. *Green Chem*, 2011, vol. 13, no. 10, pp. 2638–2650. doi:10.1039/C1GC15386B.

[9] Shankar SS, Rai A, Ahmad A, Sastry M. Rapid synthesis of Au, Ag, and bimetallic Au core–Ag shell nanoparticles using Neem (Azadirachta indica) leaf broth. *J Colloid Interface Sci*, 2004, vol. 275, no. 2, pp. 496–502. doi:10.1016/j.jcis.2004.03.003.

[10] Luther E.M., Koehler Y., Diendorf J., Epple M., Dringen R. Accumulation of silver nanoparticles by cultured primary brain astrocytes. *Nanotechnology*, 2011, vol. 22, no. 37, article number 375101. doi:10.1088/0957-4484/22/37/375101.

[11] Park M.V., Neigh A.M., Vermeulen J.P., de la Fonteyne L.J., et al. The effect of particle size on the cytotoxicity, inflammation, developmental toxicity and genotoxicity of silver nanoparticles. *Biomaterials*, 2011, vol. 32, no. 36, pp. 9810–9817. doi:10.1016/j.biomaterials.2011.08.085.

[12] Kim T.H., Kim M., Park H.S., Shin U.S., *et al*. Size-dependent cellular toxicity of silvernanoparticles. *Journal of Biomedical Materials Research – Part A*, 2012, vol. 100, no. 4, pp. 1033–1043. doi:10.1002/jbm.a.34053.

[13] Mart ınez-Casta non G.A., Ni no-Martınez N., Martınez-Gutierrez F., Martınez-Mendoza J.R., Ruiz F. Synthesis and antibacterial activity of silver nanoparticles with different sizes. *Journal of Nanoparticle Research*, 2008, vol. 10, no. 8, pp.1343–1348. doi:10.1007/s11051-008-9428-6.

[14] Kirby-Bauer A. Antimicrobial sensitivity testing by agar diffusion method. *J Clincal Pathol*., 1996, vol. 44, pp. 493–502.

[15] Shameli K., *et al*. Green biosynthesis of silver nanoparticles using Callicarpa maingayi stem bark extraction. *Molecules*, 2012, vol. 17, no. 7, pp. 8506–8517. doi: 10.3390/molecules17078506.

[16] Krishnaraj C., Jagan EG., Rajasekar S., Selvakumar P., *et al*. Synthesis of silver nanoparticles using Acalypha indica leaf extracts and its antibacterial activity against water borne pathogens. *Colloids Surf B Biointerfaces*, 2010, vol. 76, no. 1, pp. 50–56. doi: 10.1016/j.colsurfb.2009.10.008.

[17] Raja S., Ramesh V., *et al*. Green biosynthesis of silver nanoparticles using Calliandra haematocephala leaf extract, their antibacterial activity and hydrogen peroxide sensing capability. *Arab J Chem*, 2017, vol. 10, no. 2, pp. 253–261. doi: 10.1016/j.arabjc.2015.06.023.

[18] Kaur G., Athar M., Alam M.S. Quercus infectoria galls possess antioxidant activity and abrogates oxidative stress-induced functional alterations in murine macrophages. *Chem Biol Interact*, 2008, vol. 171, no. 3, pp. 272–282. doi: 10.1016/j.cbi.2007.10.002.

[19] Kaur G., Hamid H., Ali A., Alam M.S., Athar M. Antiinflammatory evaluation of alcoholic extract of galls of Quercus infectoria. *J. Ethanol.Pharm*, 2004, vol. 90, no. 2–3, pp. 285–292. doi:10.1016/j.jep.2003.10.009.

[20] Sawangjaroen N., Sawangjaroen K., Poonpanang K. Effects of Piper longum fruit, Piper sarmentosum root and Quercus infectoria nut gall on caecal amoebiasis in mice, *J. Ethanopharmacology*, 2004, vol. 91, no. 2–3, pp. 357–360. doi: 10.1016/j.jep.2004.01.014.

[21] Yousef Elahi M., Rouzbehan Y. Characteriztion of Quercus persica, Quercus infectoria and Quercus libani as ruminant feeds. *Anim Feed Sci Technol*, 2008, vol. 140, no. 1–2, pp. 78–89. doi: 10.1016/j.anifeedsci.2007.02.009.

[22] Kuo P., Yang M., Wu P., Shih H., Dinh T. Chemical constituents from Abutilon indicum. *J Asian Nat Prod Res*, 2017, vol. 10, no. 7, pp. 689–693. doi:10.1080/10286020802016545.

[23] Kalemba D., Kunicka A. Antibacterial and antifungal properties of essential oils. *Curr Med Chem*, 2003, vol. 10, no. 10, pp. 813–829. doi: 10.2174/0929867033457719.

[24] Shankar T., Karthiga P., Swarnalatha K., Rajkumar K. Green synthesis of silver nanoparticles using Capsicum frutescence and intensified activity against. *Resource Efficient Technologies*, 2017, vol. 3, no. 3, pp.303–308. 10.1016/j.reffit.2017.01.004.

[25] Santheraleka R., *et al.* Eco-friendly synthesis of *Solanum trilobatum* extract-capped silver nanoparticles is compatible with good antimicrobial activities. *J Mol Struct*, 2018, vol. 1160, pp. 80–91. doi: 10.1016/j.molstruc.2018.01.056

[26] Powers C.M., Badireddy A.R., Ryde I.T., Seidler F.J., Slotkin T.A. Silver nanoparticles compromise neurodevelopment in PC12 cells: critical contributions of silver ion, particle size, coating, and composition. *Environ Health Perspect*, 2011, vol. 119, no.1, pp. 37–44. doi:10.1289/ehp.1002337.

[27] Gorth DJ., Webster TJ. Silver nanoparticle toxicity in Drosophila: size does matter. *Int J Nanomed*, 2011, vol. 6, pp. 343–350. doi: 10.2147/IJN.S16881.

[28] Muhammad S.U., *et al.* Synthesis, characterization, and antimicrobial properties of copper nanoparticles. *Int. J. Nanomed.*, 2013, vol. 8, pp. 4467–4479. doi: 10.2147/IJN.S50837.

[29] Krishnaraj C., Muthukumaran P., Ramachandran R., Balakumaran M.D., Kalaichelvan P.T. Acalypha indica Linn: biogenic synthesis of silver and gold nanoparticles and their cytotoxic effects against MDA-MB-231, human breast cancer cells. *Biotechnol Rep*, 2014, vol. 4, no.1, pp. 42–49. doi: 10.1016/j.btre.2014.08.002.

[30] Senthilraja P and Kathiresan K. In vitro cytotoxicity MTT assay in Vero, HepG2 and MCF -7 cell lines study of Marine Yeast. *J App Pharm Sci*, 2015, vol. 5, no. 3, pp. 80–84. doi: 10.7324/JAPS.2015.50313.

[31] Murugan K., *et al.* Hydrothermal synthesis of titanium dioxide nanoparticles: mosquitocidal potential and anticancer activity on human breast cancer cell line (MCF-7). *Parasitology Res*, 2016, vol. 115, no. 3, pp. 1085–1096. doi: 10.1007/s00436-015-4838-8.

*Received: December 12, 2019*